

A synthetic tryptophan metabolite reduces hemorrhagic area and inflammation after pulmonary radiofrequency ablation in rabbit non-neoplastic lungs.

Hiroshi Nakada • Atsushi Yamashita • Masaomi Kuroki • Eiji Furukoji • Noriko Uchino
• Taketoshi Asanuma • Yujiro Asada • Shozo Tamura

Department of Radiology (H.N., E.F, N.U., S.T.), Department of Pathology (A.Y., Y.A.), Faculty of Medicine; Department of Veterinary Sciences, Faculty of Agriculture (T.A.), University of Miyazaki, 5200 Kihara, Kiyotake, Miyazaki 889-1692, Japan

Department of Radiology (M.K.), Fujimoto Central Hospital, 3584-1, Ranbashi, kitakawauchi, Miyazaki City, Miyazaki 880-0941, Japan

Conflict of Interest: None

Corresponding author:

Hiroshi Nakada

Department of Radiology, Faculty of Medicine, University of Miyazaki, 5200 Kihara, Kiyotake, Miyazaki 889-1692, Japan

Telephone: +81-985-85-2807; Fax: +81-985-85-3392

E-mail: nkdhrs@med.miyazaki-u.ac.jp

* This research was supported in part by a Grants-in-Aid for Scientific Research in Japan (Nos. 19790885 H.N., 23790410, 25460440 A.Y., 23390084 Y.A.)

Abstract

Purpose: The purpose of this study was to determine the effect of a synthetic tryptophan metabolite, tranilast [N-(3,4-dimethoxycinnamoyl)-anthranilic acid], on inflammatory and hemorrhagic areas after pulmonary radiofrequency ablation (RFA) in rabbits.

Materials and methods: Percutaneous RFA using a 17-gauge LeVein electrode was performed in normal rabbit lungs. The rabbits were divided into tranilast-treated (300 mg/kg/day, orally) and control groups (n = 24 /group). The effects of tranilast were evaluated using multidetector-row computed tomography (CT), histology, and immunohistochemistry immediately after RFA on days 1, 7, 14, and 28.

Results: Oral administration of tranilast significantly reduced the size of ablated lesions assessed using CT and histology on days 7 and 14. Furthermore, it reduced the hemorrhagic areas on day 7 and inflammatory areas on day 14, but did not affect the areas of coagulation necrosis on days 1, 7, 14, and 28. Immunohistochemical analysis showed an increase in the ratio of CD163-positive macrophage areas to RAM11-positive pan-macrophage areas and a decrease in the number of nuclear factor- κ B-positive nuclei and CD31-positive microvessels in the tranilast group on days 7 and/or 14.

Conclusions: The results suggest that tranilast modulates the repair process after pulmonary RFA through macrophage accumulation, suppression of inflammation, and angiogenesis.

Keywords: lungs, radiofrequency ablation, inflammation, CD163, tranilast

Introduction

Radiofrequency ablation (RFA) has emerged as an alternative for patients who are ineligible for surgery, and it can locally control and palliate primary and secondary tumors in various organs, including the lungs [1]. Although several clinical trials have shown that pulmonary RFA is safe and is related to promising long-term survival outcomes [2-4], some patients (32% - 42%) still remain at risk of local recurrence [5-7]. To decrease the risk of incomplete ablation, ablation using a 1-cm margin at the periphery of the tumor is considered the standard practice [5, 8, 9]. However, the ablated area assessed using multidetector-row computed tomography (CT) will continue to be larger than the original size, as a result of response to thermal injury, e.g. peripheral parenchymal edema, inflammation, and hemorrhage in the acute to intermediate phase after RFA [9]. Ablation-related inflammatory changes are detected by ¹⁸F-fluorodeoxyglucose positron emission tomography (PET) in normal surrounding tissues [10]. Thus, sustained inflammation due to RFA may cause problems for early assessment of treatment effects. It is important to distinguish thermally damaged normal tissues from residual tumor in the early stage after RFA. Therefore, reducing inflammatory changes after RFA is considered to be beneficial for assessing the effects.

Tranilast [N-(3, 4-dimethoxycinnamoyl)-anthranilic acid] is a synthetic tryptophan metabolite that exhibits anti-inflammatory and immunomodulatory effects. It has been clinically used as an oral anti-allergic drug for nearly three decades in Japan for treatment of diseases such as bronchial asthma, allergic rhinitis and atopic dermatitis [11, 12]. The effects of tranilast are considered to be mediated by inhibition of the release of chemical mediators and cytokines from mast cells and basophils [11]. Recent studies have further revealed that tranilast inhibits the expression of many cytokines,

chemokines, and proteases in various cell types including fibroblasts, lymphocytes, macrophages and neutrophils [13-15]. In addition to its anti-inflammatory effects, tranilast has been shown to modulate functions of smooth muscle cell (SMC)s, myofibroblasts, or endothelial cells [16-19].

In this study, we examined the effects of tranilast on the repair process in normal rabbit lungs after pulmonary RFA.

Materials and methods

Animals and setting

The Animal Care Committee of our institution approved the animal research protocols of the present prospective study, which also conformed to the Guide for the Care and Use of Laboratory Animals published by the US National Institutes of Health.

Three-month-old Japanese white rabbits (n = 48) weighing 2.5 – 3.0 kg were used to study the process of lung damage after RFA. The rabbits were randomly divided into two groups (n = 24 each): the control group (standard chow containing placebo) and the tranilast-treated group (standard chow containing tranilast). Tranilast powder (Kissei Pharmaceutical Co., Ltd., Nagano, Japan) was mixed with the pelleted diet at an oral dose of 300 mg/kg/day from the day before RFA. This dose was selected because its oral administration maintained plasma concentrations of tranilast at 10 - 100 $\mu\text{mol/L}$, which have an anti-immunological activation in rabbits [19, 20].

Study protocol and RFA procedures

The rabbits were subcutaneously administered medetomidine hydrochloride (0.1 mg/kg, Domitor; Orion Pharma, Espoo, Finland). General anesthesia was induced by intravenous (i.v.) administration of pentobarbital sodium (25 mg/kg Nembutal; Dainippon Sumitomo Pharma Co. Ltd., Osaka, Japan).

Array-style 17-gauge LeVeen radiofrequency ablation electrodes, 2.0 cm in diameter, (Boston Scientific, Boston, MA, USA) and a radiofrequency generator (RF2000; Boston Scientific) were percutaneously placed into the lung under CT guidance (LightSpeed16; GE Healthcare, Milwaukee, WI, USA). The electrode tines were minimally expanded to 1 cm in diameter to generate a single heating point (Figs. 1). The ablation protocol consisted of an initial 5-W power setting with an increase of 5 W/min. The manufacturer's instructions for use of the device consider ablation to be complete if the current precipitously decreases or impedance increases (roll-off). RFA application to the same position was repeated after a 30-s interval until roll-off occurred [21]. Therapeutic aspiration procedure using a 23-G aspirating needle was performed under CT guidance when severe pneumothorax occurred after RFA.

A sequential CT evaluation was performed in eight rabbits (n = 4 in each group) on days 0 and 1 (acute phase), on days 7 and 14 (subacute phase), and on days 21 and 28 (chronic phase). These rabbits were sacrificed on days 28 for histological evaluation. The other 40 rabbits were used for only histological evaluation on days 1, 7, 14 (n = 6 in each group) and 28 (n = 2 in each group) after RFA procedure. The rabbits were sacrificed by administering an overdose of pentobarbital (60 mg/kg, intravenously).

Venous blood samples were collected on days 0, 1, 7, and 14. We measured the leukocyte count (KX-21; Sysmex, Kobe, Japan) and serum levels of C-reactive protein

(Rabbit CRP ELISA KIT; Shibayagi, Gunma, Japan).

Follow-up CT imaging

A multidetector-row CT scanner (LightSpeed16; GE Healthcare) was used to perform CT to monitor the ablation effects immediately after RFA (day 0) and on days 1, 7, 14, 21, and 28 throughout each experimental period, with the rabbits under sedation by administration of medetomidine hydrochloride. The following CT scan parameters were used: 100–150 mA, 120 kV, 1.25-mm collimation with 1.25-mm reconstruction, and a 120-mm field of view. A workstation equipped with software (ZIOSTATION; AMIN, Tokyo, Japan) was used to measure the volume (mm^3) of ablated lesions on the CT scans by two investigators who were blinded for the study purpose. We defined the ablated lesion according to the radiological criteria [9, 22]. The lesion on CT was showed as an extensive area of ground-glass opacity on days 0 and 1, and showed as a well demarcated dense opacity excluding adjacent structures (blood vessels, chest wall) and unrelated disease such as atelectasis and consolidation on days 7, 14, 21 and 28.

Microscopic findings

After the experimental period, an extension tube (12 Fr.) was used to isolate and inflate the ablated lungs with air to maintain antemortem lung volumes. Next, a central cross-sectional incision was made through the affected area, and 5-mm-thick serial sections were made from the lesion to provide the same sectioning as that used in CT. These lung tissue samples were fixed in 4% paraformaldehyde at 4°C overnight and

embedded in paraffin; thin-sliced sections (3- μm thick) were stained with hematoxylin and eosin, and Sirius red staining was used for histological evaluation and analysis of collagen fibers.

Image processing software (WinROOF; Mitani, Fukui, Japan) was used to measure the maximum areas (mm^2) of RFA on microscopic digital images by two investigators who were blinded for the study purpose. Histologically, we defined the ablated areas as reported previously [21, 23]. The ablated area consisted of multi-layered structures of coagulation necrosis, hemorrhage, peripheral inflammatory reaction, or fibrous tissue depending on the time after RFA. To evaluate the effects of tranilast, the areas of the layers were calculated for each group.

Immunohistochemical findings

The sections (3- μm thick) were stained and immunohistochemically examined using antibodies against nuclear factor- κB (NF- κB ; Abnova, Taiwan), rabbit macrophages (RAM11; DAKO, Japan), CD163 (a marker of M2 macrophages, AM3K; Transgenic, Japan) [24], CD31 (a marker of vascular endothelial cells; DAKO, Japan), and muscle actin (a marker of SMCs and myofibroblasts, HHF35; DAKO, Japan). Two investigators (blinded for the study purpose) used color imaging morphometry system (WinROOF, Mitani, Fukui, Japan) to semiquantify the immunopositive areas for RAM11, CD163, and HHF35 [25]. The percentages of CD163-positive cell (M2 macrophage) areas in RAM11-positive cell (pan-macrophage) areas were calculated by dividing the CD163-positive cell area with the RAM11-positive cell area in the adjacent sections. The number of immunopositive nuclei for NF- κB and CD31-positive

microvessels were counted at the peripheral inflammatory lesions, and the densities were expressed as the number of nuclei or microvessels per mm².

Statistical analysis

All data are presented as mean \pm standard deviation. Two-way ANOVA or Mann Whitney U-test (GraphPad Prism 5.01; GraphPad Software Inc., San Diego, CA, USA) was used to test differences between the groups. A value of $P < 0.05$ was considered to indicate statistical significance.

Results

RFA lesion size and pathological findings

CT-guided RFA was successfully performed in all 48 rabbits with normal lungs (Fig. 1). Roll-off was reached in 122 ± 30 s, on average, during the first ablation. The mean baseline impedance was $181.6 \pm 41 \Omega$, and the mean maximum power output was 11.7 ± 2.6 W. There were no significant differences in these RFA procedure parameters between the two groups. The leukocyte counts and serum levels of CRP increased on day 1, however, there were no significant differences between the groups (leukocyte counts, control group: $6000 \pm 700 /\mu\text{L}$, tranilast-treated group: $6700 \pm 100 /\mu\text{L}$, $P = 0.24$, $n = 4$ each; serum CRP levels, control group: 6.6 ± 6.0 mg/dL, tranilast -treated group: 7.3 ± 2.6 mg/dL, $P = 0.89$, $n = 4$ each)

Pneumothorax was observed immediately after RFA in one rabbit for CT evaluation.

The lung was aerated about ten minute after aspiration procedure, and its CT image was hardly affected.

Sequential CT volumetry (Figs. 1, 2a) demonstrated that administration of tranilast significantly reduced the lesion size, particularly on days 7 and 14. Coincident with the CT findings, the pathological areas of the ablated lungs (Fig. 2b) were significantly different on days 7 and 14.

In the acute phase after RFA, the lung lesions appeared as ground-glass opacity (GGO) areas on the CT images (Fig. 1). There were no significant differences in the CT volumes and pathological areas between the two groups in the acute phase on day 1 (Fig. 2). Histologically, the ablated areas consisted of two microscopic layers on day 1 (data not shown). Massive coagulation necrosis with effusion was located in the inner layer. Alveolar effusion, fibrin exudates, and congestion were seen in the outer layer. The alveolar structure and cell nuclei were apparently retained. There were no significant differences in the areas of coagulation necrosis (control group: $23 \pm 4 \text{ mm}^2$, tranilast-treated group: $27 \pm 7 \text{ mm}^2$, $P = 0.48$, $n = 6$ each) and the congestive areas (control group: $36 \pm 21 \text{ mm}^2$, tranilast-treated group: $25 \pm 7 \text{ mm}^2$, $P = 0.59$, $n = 6$ each).

In the subacute phase after RFA on days 7 and 14, the CT images for the lung lesions appeared as solid nodules with or without inner GGO layers (Fig. 1). Histologically, the ablated areas consisted of three microscopic layers of coagulation necrosis, hemorrhage, and inflammatory reaction on day 7 (Fig. 3a), and consisted of coagulation necrosis with hemorrhage, and inflammatory reaction with fibrous granulation tissue on day 14 (Fig. 4a) [21, 23]. On day 7, the hemorrhagic area was significantly smaller in the tranilast-treated group than that of the control group (Fig. 3c). On day 14, the areas of peripheral inflammatory reaction were significantly smaller than those of the control

group (Fig. 4c).

In the chronic phase on day 28, the lung lesions appeared as solid nodules that gradually decreased in size (Fig. 1). The CT volumes and pathological areas tended to be smaller in the tranilast-treated group than those of control groups; however, there were no significant differences between the two groups (Fig. 2, CT volumes: $P = 0.09$, pathological areas: $P = 0.09$). In addition, analysis using Sirius red stain of the fibrotic areas in the chronic phase did not show a significant difference (day 28; control group: 3.3 ± 1.1 %, tranilast-treated group: 3.1 ± 0.9 %, $P = 0.81$, $n = 6$ in each group).

Immunohistochemical findings

Immunohistochemical staining showed an infiltrate of RAM11-positive pan-macrophages and CD163-positive macrophages in the ablated lesions (Fig. 5). Both positive areas peaked on day 14. The RAM11-positive area was significantly smaller in the tranilast-treated group on days 7 and 14. The ratio of the CD163-positive macrophage area to the RAM11-positive pan-macrophage area (Figs. 5, 6) was significantly higher in the tranilast-treated group than in the control group on days 7 and 14 (Fig. 6). Similar to the observations for the macrophage contents, the number of NF- κ B-positive nuclei and the microvessel density peaked on day 14, and the number of NF- κ B-positive nuclei was significantly lower on day 7, and the CD31 microvessel density was significantly lower on day 14 in the tranilast-treated group than in the control group (Fig. 6). There were no significant differences in the percentages of HHF35-positive SMC / myofibroblast areas between the two groups (Fig. 6).

Discussion

The present study demonstrated that oral administration of tranilast reduced inflammatory reactions and hemorrhagic areas in normal rabbit lungs after RFA, in addition, the administration of tranilast increased the content of CD163-positive macrophages.

PET and CT are imaging modalities for post-RFA follow up. However, the appropriate follow-up initiation time point for PET is also at least three months following RFA to avoid false positives that are caused by persistent inflammation in the outer zone [26]. On contrast-enhanced CT, benign periablational enhancements may persist for as long as six months after RFA [9]. The increasing contrast material uptake reflects vascularity of the lesion rather than neoplastic proliferation. The inflammatory reaction after lung RFA may cause problems for assessment of treatment effects and complications such as fever, hemoptysis, and obstructive pneumonia [27]. Tranilast, a tryptophan metabolite analog, is currently used to treat allergy (type 1 hypersensitivity) [11] and keloid [17]. It has other biological effects including inhibition of leukotrienes, cytokines, prostaglandins, and oxygen radicals [28, 29]. Compared with other anti-inflammatory agents, such as corticosteroids, tranilast lacks serious adverse effects, which allows its long-term administration. Therefore, tranilast may be beneficial in anti-inflammatory treatment after lung RFA.

CD163 is a scavenger receptor for haptoglobin–hemoglobin complexes, and seems to be a useful marker for anti-inflammatory M2 macrophages [24]. After uptake of the haptoglobin–hemoglobin complex by CD163, liberated heme is converted into less toxic compounds, such as ferrous ion, carbon monoxide, and biliverdin–bilirubin, by

heme oxygenase 1 [30]. Therefore, the enhanced accumulation of CD163 macrophage in the tranilast-treated group may be a favorable finding for reduction of heme-induced oxidative stress. Tranilast increased production of interleukin (IL)-4 and IL-10 [13]. Because these cytokines mediate M2 macrophage polarization [31], it is possible that the immunomodulatory effect of tranilast enhances accumulation of CD163 macrophages. The reduction of hemorrhagic area in the tranilast-treated group could be partly explained by accumulation of hemoglobin scavenging CD163 macrophages in the ablated lesions. Whether the hemorrhagic area only involves inflammation or has some necrotic parts is controversial. Although we cannot conclude whether this is due to reduced hemorrhaging or enhanced resolution of the hemorrhagic area, the increase in the ratio of CD163-positive macrophages in the tranilast-treated group suggests that the latter is probable.

The oral administration of tranilast reduced peripheral inflammatory reaction after RFA. As previously reported [23, 32], the necrotic lung parenchyma after RFA showed hemorrhagic necrosis at the marginal portion of lesions, and this portion was gradually replaced by inflammatory granulation tissue and fibrous tissue. In addition to hemoglobin scavenging, M2 macrophages have an important role in wound healing and tissue repair and turn off immune system activation by producing anti-inflammatory cytokines, such as IL-10 [24]. NF- κ B can affect pulmonary inflammation, cell proliferation and survival, and angiogenesis in pulmonary diseases [33]. Tranilast inhibited cytokine-induced NF- κ B activation in cultured human umbilical vein endothelial cells [34]. Moreover, tranilast inhibited proliferation of human dermal endothelial cells and angiogenesis in vivo [18]. Although the precise mechanisms remain unknown, the reduction of peripheral inflammatory reactions in the

tranilast-treated group might be partly due to tranilast's effect on macrophages, NF- κ B activation, and endothelial cells.

In contrast to our results, previous studies demonstrated that tranilast prevents migration, proliferation, and collagen synthesis of cultured SMCs, and proliferation of fibroblasts [16, 17, 20]. Moreover, tranilast suppressed formation of SMC-rich intimal lesions after directional coronary atherectomy in patients with coronary stenosis [35]. Although we cannot clearly explain this discrepancy, it could be because of the differences in tissues and organs and stimulation of inflammation.

Our study had several limitations. We examined RFA lesions in non-neoplastic rabbit lungs to evaluate the effect of tranilast on a repair process after RFA. Because the roles of tumor-associated macrophages in non-small cell lung cancer have been shown to be conflicting [36, 37], it is unclear whether enhanced accumulation of CD163 macrophages in RFA lesions promotes tumor recurrence. In addition, the reduction of microvessel density could be a favorable finding for preventing tumor recurrence. Further examinations with a neoplastic lung model are required to evaluate whether tranilast can actually reduce complications and the number of false positive cases after RFA for human lung tumors. Although CT imaging was not performed during breath holds, high-quality imaging with high-speed multidetector CT and sedation allowed measurement of the ablated lesion volumes.

We could not measure a plasma concentration of tranilast throughout the period of the experiment. Previous studies showed that its oral dose of 300 mg/kg/day, a same dose in this study, maintained tranilast plasma concentrations at 10 - 100 μ mol/L, which have an anti-immunological action in vitro and in vivo experiment [19, 20]. These reports suggest that this dose of tranilast would be affective in this study.

In conclusion, we demonstrated that tranilast modulated the repair process after pulmonary RFA through CD163-positive macrophage accumulation and reduced inflammation and angiogenesis in normal rabbit lungs. The present findings could provide valuable information that may be helpful for further experiments of tumor models and clinical trial for human lung tumors.

References

1. Gazelle GS, Goldberg SN, Solbiati L, Livraghi T. Tumor ablation with radio-frequency energy. *Radiology*. 2000; 217:633-46.
2. Simon CJ, Dupuy DE, DiPetrillo TA, Safran HP, Grieco CA, Ng T., et al. Pulmonary radiofrequency ablation: long-term safety and efficacy in 153 patients. *Radiology*. 2007; 243:268-75.
3. Kelekis AD, Thanos L, Mylona S, Ptohis N, Malagari K Nikita, A., et al. Percutaneous radiofrequency ablation of lung tumors with expandable needle electrodes: current status. *Eur Radiol*. 2006; 16:2471-82.
4. Wolf FJ, Grand DJ, Machan JT, Dipetrillo TA, Mayo-Smith WW, Dupuy DE. Microwave ablation of lung malignancies: effectiveness, CT findings, and safety in 50 patients. *Radiology*. 2008; 247:871-9.
5. Beland MD, Wasser EJ, Mayo-Smith WW, Dupuy DE. Primary non-small cell lung cancer: review of frequency, location, and time of recurrence after radiofrequency ablation. *Radiology*. 2010; 254:301-7.
6. Okuma T, Matsuoka T, Yamamoto A, Oyama Y, Hamamoto S, Toyoshima M., et al. Determinants of local progression after computed tomography-guided percutaneous radiofrequency ablation for unresectable lung tumors: 9-year experience in a single institution. *Cardiovasc Intervent Radiol*. 2010; 33:787-93.
7. Hiraki T, Sakurai J, Tsuda T, Gohara H, Sano Y, Mukai T., et al. Risk factors for local progression after percutaneous radiofrequency ablation of lung tumors: evaluation based on a preliminary review of 342 tumors. *Cancer*. 2006; 107:2873-80.

8. Giraud P, Antoine M, Larrouy A, Milleron B, Callard P, De Rycke Y., et al. Evaluation of microscopic tumor extension in non-small-cell lung cancer for three-dimensional conformal radiotherapy planning. *Int J Radiat Oncol Biol Phys.* 2000; 48:1015-24.
9. Abtin FG, Eradat J, Gutierrez AJ, Lee C, Fishbein MC, Suh RD. Radiofrequency ablation of lung tumors: imaging features of the postablation zone. *Radiographics.* 2012; 32:947-69.
10. Okuma T, Matsuoka T, Okamura T, Wada Y, Yamamoto A, Oyama Y., et al. ¹⁸F-FDG small-animal PET for monitoring the therapeutic effect of CT-guided radiofrequency ablation on implanted VX2 lung tumors in rabbits. *J Nucl Med.* 2006; 47:1351-8.
11. Azuma H, Banno K, Yoshimura T. Pharmacological properties of N-(3',4'-dimethoxycinnamoyl) anthranilic acid (N-5'), a new anti-atopic agent. *Br J Pharmacol.* 1976; 58:483-488.
12. Koda A, Nagai H, Watanabe S, Yanagihara Y, Sakamoto K. Inhibition of hypersensitivity reactions by a new drug, N-(3',4'-dimethoxycinnamoyl) anthranilic acid (N-5'). *J Allergy Clin Immunol.* 1976; 57:396-407.
13. Platten M, Ho PP, Youssef S, Fontoura P, Garren H, Hur EM., et al. Treatment of autoimmune neuroinflammation with a synthetic tryptophan metabolite. *Science.* 2005; 310:850-855.
14. Chikaraishi A, Hirahashi J, Takase O, Marumo T, Hishikawa K, Hayashi M., et al. Tranilast inhibits interleukin-1beta-induced monocyte chemoattractant protein-1 expression in rat mesangial cells. *Eur J Pharmacol.* 2001; 427:151-8.

15. Shimizu T, Kimura T, Funahashi T, Watanabe K, Ho IK, Yamamoto I. Displacement of opioid receptor binding ligands from the rat brain by N3-(2',5'-dimethoxyphenacyl) arabinofuranosyluracil. *Res Commun Mol Pathol Pharmacol.* 2005; 117-118:105-13.
16. Sata M, Takahashi A, Tanaka K, Washida M, Ishizaka N, Ako J., et al. Mouse genetic evidence that tranilast reduces smooth muscle cell hyperplasia via a p21(WAF1)-dependent pathway. *Arterioscler Thromb Vasc Biol.* 2002; 22:1305-9.
17. Isaji M, Nakajoh M, Naito J. Selective inhibition of collagen accumulation by N-(3,4-dimethoxycinnamoyl)anthranilic acid (N-5') in granulation tissue. *Biochem Pharmacol.* 1987; 36:469-74.
18. Isaji M, Miyata H, Ajisawa Y, Takehana Y, Yoshimura N. Tranilast inhibits the proliferation, chemotaxis and tube formation of human microvascular endothelial cells in vitro and angiogenesis in vivo. *Br J Pharmacol.* 1997; 122:1061-6.
19. Matsumura T, Kugiyama K, Sugiyama S, Ota Y, Doi H, Ogata N., et al. Suppression of atherosclerotic development in Watanabe heritable hyperlipidemic rabbits treated with an oral antiallergic drug, tranilast. *Circulation.* 1999; 99:919-4.
20. Fukuyama J, Ichikawa K, Miyazawa K, Hamano S, Shibata N, Ujiie A. Tranilast suppresses intimal hyperplasia in the balloon injury model and cuff treatment model in rabbits. *Jpn J Pharmacol.* 1996; 70:321-7.
21. Kuroki M, Nakada H, Yamashita A, Sawaguchi A, Uchino N, Sato S., et al. Loss of cellular viability in areas of ground-glass opacity on computed tomography images immediately after pulmonary radiofrequency ablation in rabbits. *Jpn J Radiol.* 2012; 30:323-30.

22. Tominaga J, Miyachi H, Takase K, Matsushashi T, Yamada T, Sato A., et al. Time-related changes in computed tomographic appearance and pathologic findings after radiofrequency ablation of the rabbit lung: preliminary experimental study. *J Vasc Interv Radiol.* 2005; 16:1719-26.
23. Yamamoto A, Nakamura K, Matsuoka T, Toyoshima M, Okuma T, Oyama Y., et al. Radiofrequency ablation in a porcine lung model: correlation between CT and histopathologic findings. *AJR Am J Roentgenol.* 2005; 185:1299-306.
24. Komohara Y, Hirahara J, Horikawa T, Kawamura K, Kiyota E, Sakashita N., et al. AM-3K, an anti-macrophage antibody, recognizes CD163, a molecule associated with an anti-inflammatory macrophage phenotype. *J Histochem Cytochem.* 2006; 54:763-71.
25. Yamashita A, Matsuda S, Matsumoto T, Moriguchi-Goto S, Takahashi M, Sugita C., et al. Thrombin generation by intimal tissue factor contributes to thrombus formation on macrophage-rich neointima but not normal intima of hyperlipidemic rabbits. *Atherosclerosis.* 2009; 206:418-26.
26. Higaki F, Okumura Y, Sato S, Hiraki T, Gobara H, Mimura H., et al. Preliminary retrospective investigation of FDG-PET/CT timing in follow-up of ablated lung tumor. *Ann Nucl Med.* 2008; 22:157-63.
27. Lee JM, Jin GY, Goldberg SN, Lee YC, Chung GH, Han YM., et al. Percutaneous radiofrequency ablation for inoperable non-small cell lung cancer and metastases: preliminary report. *Radiology.* 2004; 230:125-34.
28. Komatsu H, Kojima M, Tsutsumi N, Hamano S, Kusama H, Ujiie A, et al. Mechanism of inhibitory action of tranilast on the release of slow reacting substance

- of anaphylaxis (SRS-A) in vitro: effect of tranilast on the release of arachidonic acid and its metabolites. *Jpn J Pharmacol.* 1988; 46:53-60.
29. Komatsu H, Kojima M, Tsutsumi N, Hamano S, Kusama H, Ujiie A, et al. Study of the mechanism of inhibitory action of tranilast on chemical mediator release. *Jpn J Pharmacol.* 1988; 46:43-51.
30. Martin-Ventura JL, Madrigal-Matute J, Martinez-Pinna R, Ramos-Mozo P, Blanco-Colio LM, Moreno JA., et al. Erythrocytes, leukocytes and platelets as a source of oxidative stress in chronic vascular diseases: detoxifying mechanisms and potential therapeutic options. *Thromb Haemost.* 2012; 108:435-42.
31. Tugal D, Liao X, Jain MK. Transcriptional control of macrophage polarization. *Arterioscler Thromb Vasc Biol;* 33:1135-1144.
32. Oyama Y, Nakamura K, Matsuoka T, Toyoshima M, Yamamoto A, Okuma T., et al. Radiofrequency ablated lesion in the normal porcine lung: long-term follow-up with MRI and pathology. *Cardiovasc Intervent Radiol.* 2005; 28: 346-53.
33. Wright JG, Christman JW. The role of nuclear factor kappa B in the pathogenesis of pulmonary diseases: implications for therapy. *Am J Respir Med.* 2003; 2:211-219.
34. Spiecker M, Lorenz I, Marx N, Darius H. Tranilast inhibits cytokine-induced nuclear factor kappaB activation in vascular endothelial cells. *Mol Pharmacol.* 2002; 62:856-863.
35. Kosuga K, Tamai H, Ueda K, Hsu YS, Ono S, Tanaka S., et al. Effectiveness of tranilast on restenosis after directional coronary atherectomy. *Am Heart J.* 1997; 134:712-8.

36. Ohri CM, Shikotra A, Green RH, Waller DA, Bradding P. The tissue microlocalisation and cellular expression of CD163, VEGF, HLA-DR, iNOS, and MRP 8/14 is correlated to clinical outcome in NSCLC. *PLoS One*; 6:e21874.
37. Carus A, Ladekarl M, Hager H, Pilegaard H, Nielsen PS, Donskov F. Tumor-associated neutrophils and macrophages in non-small cell lung cancer: No immediate impact on patient outcome. *Lung Cancer*. 2013; 81:130-7.

Figure legends

Fig. 1: Follow-up computed tomographic (CT) images of control and tranilast-treated rabbits after lung RFA over time

CT images performed immediately after RFA show a LeVeen needle positioned in the right lower lobe of the lung and ground-glass opacity around the needle (*arrows*). The electrode probe tines were half expanded to 10 mm in diameter to produce a heating point. CT images from days 7, 14, and 28 after RFA show the ablated lungs as solid nodules that decrease with time (*arrows*). On day 7, the ablated lesion of the control group contained inner GGO area (*arrow head*).

Fig. 2: The effects of tranilast on computed tomographic (CT) volumetry and on the pathological areas of the ablated lungs

(a) Graph of sequential CT volumetry shows that the administration of tranilast significantly affected the volumes of the ablated lesions ($P < 0.05$; $n = 4$ per group, two-way ANOVA) and significantly reduced the volumes lesions on days 7 and 14 ($*P < 0.05$; $n = 4$ per group, post-hoc test: Bonferroni).

(b) The pathological areas of the ablated lesions significantly differ between the control and tranilast-treated groups on days 7 and 14 ($*P < 0.05$; $n = 6$ per group, Mann Whitney U-test).

Fig. 3: Representative microscopic image of a rabbit lung on day 7 after RFA

(a) A microscopic image shows ablated areas comprising three layers: an inner coagulation necrosis (*), intermediate hemorrhagic necrosis (*arrows*), and outer

peripheral inflammatory reaction layers (*arrow heads*) (hematoxylin and eosin stain). In addition, it shows the areas of coagulation necrosis (b), hemorrhagic necrosis (c), and peripheral inflammatory reaction (d) ($*P < 0.05$; $n = 6$ per group, Mann Whitney U-test).

Fig. 4: Representative microscopic image of a lesion on day 14 after RFA

A microscopic image (a) shows the ablated areas comprising two layers: an inner coagulation necrosis mixed with hemorrhage (*) and outer peripheral inflammatory reaction layers (*arrows*) (hematoxylin and eosin stain).

Areas of coagulation necrosis mixed with hemorrhage (b) and peripheral inflammatory reaction (c) ($*P < 0.05$; $n = 6$ per group, Mann Whitney U-test).

Fig. 5: Representative immunohistochemical images of RFA lesions

Paraffin sections were immunohistochemically stained against antibodies for RAM11 (day 14), CD163 (day 14), NF- κ B (day 7), and CD31 (day 14). The administration of tranilast reduces infiltration of RAM11-positive pan-macrophage, the number of immunopositive nuclei for NF- κ B, and the number of CD31-positive microvessels, whereas the administration of tranilast enhances infiltration of CD163-positive macrophages. The images for RAM11 and CD163 show corresponding areas in serial sections.

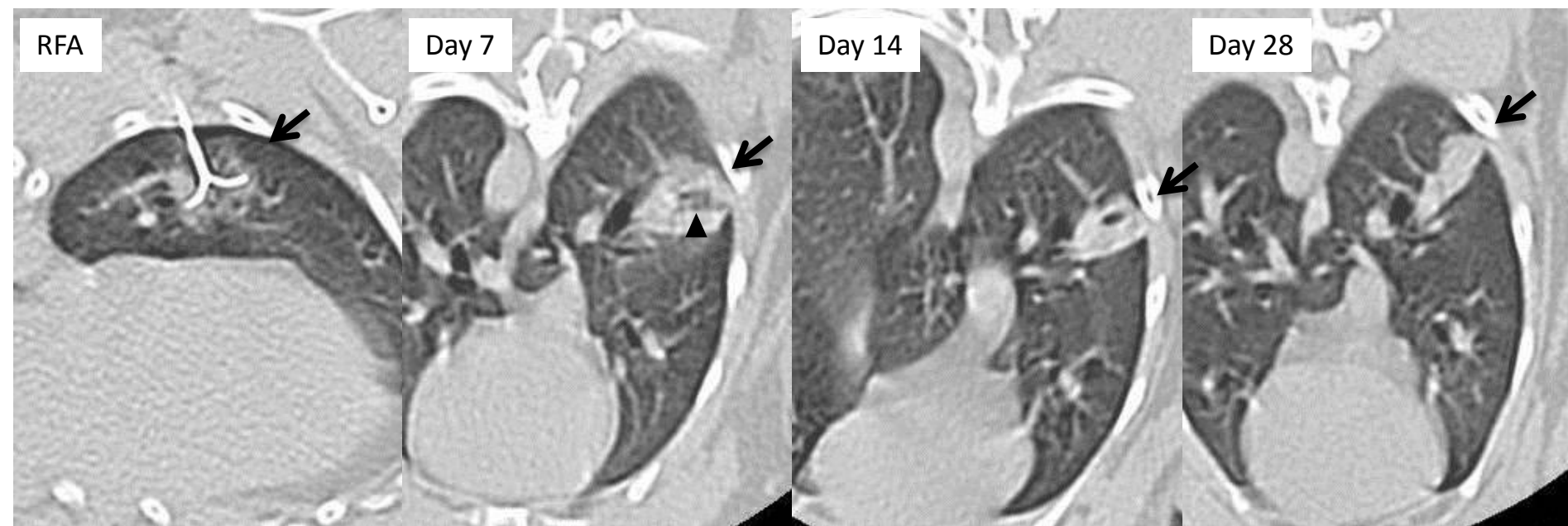
Fig. 6: Effects of tranilast on immunopositive areas in RFA lesions

Immunohistochemical analysis shows an increase in the CD163-positive macrophage areas, a decrease in RAM11-positive pan-macrophage areas, and the number of NF- κ B-

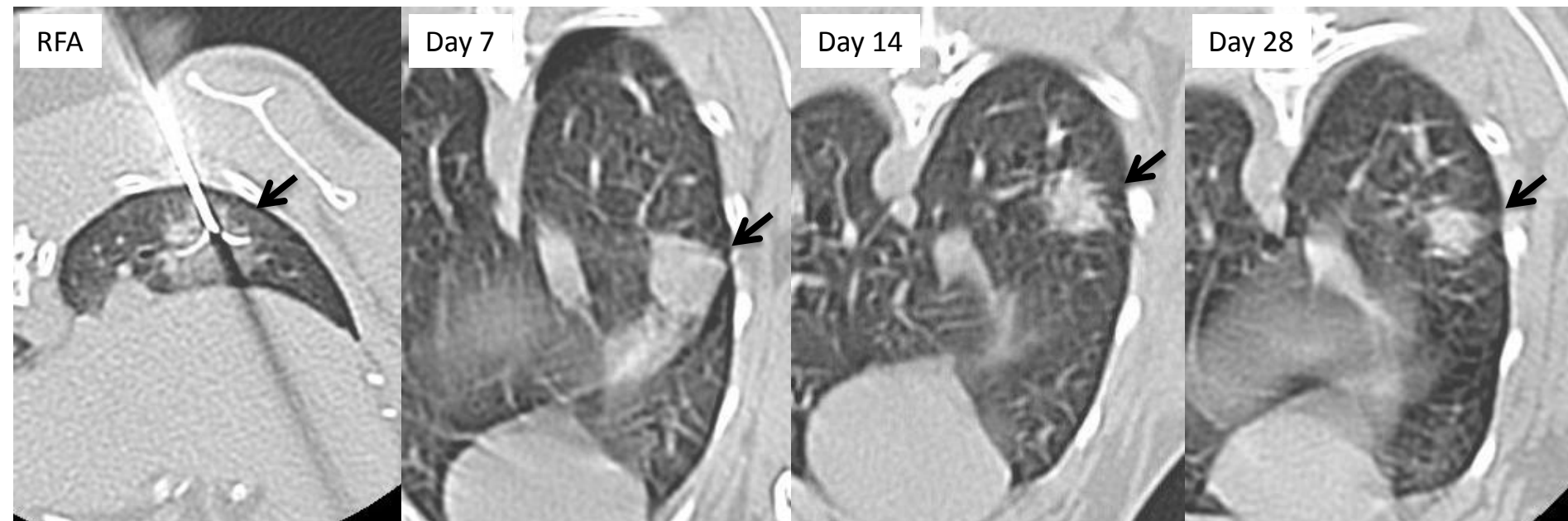
immunopositive nuclei and CD31-positive microvessel density in the tranilast group on days 7 and 14 (**** $P < 0.01$** , *** $P < 0.05$** ; n = 6 per group, Mann Whitney U-test).

Figure 1

Control rabbit

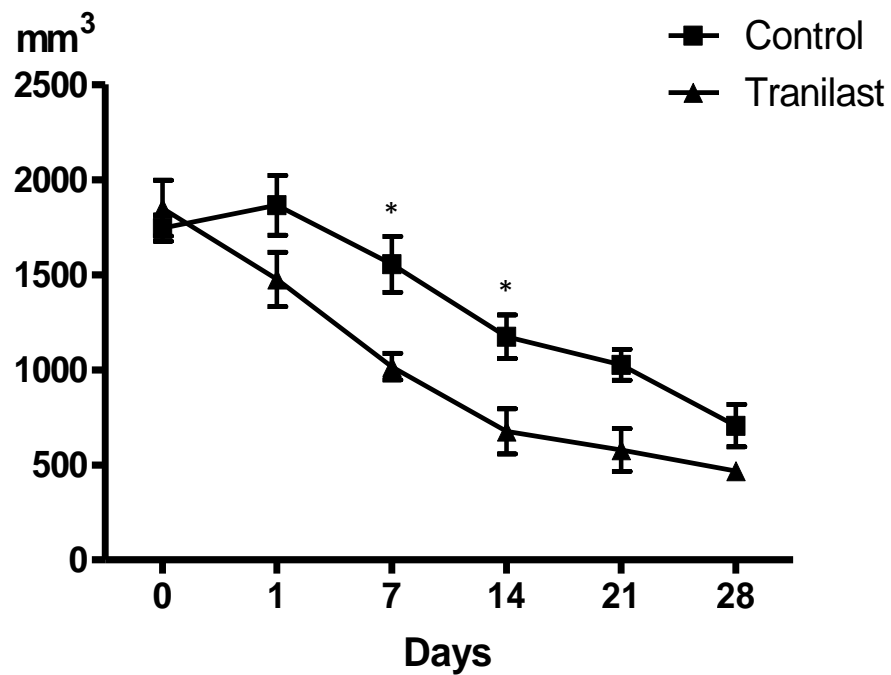


Tranilast-treated rabbit



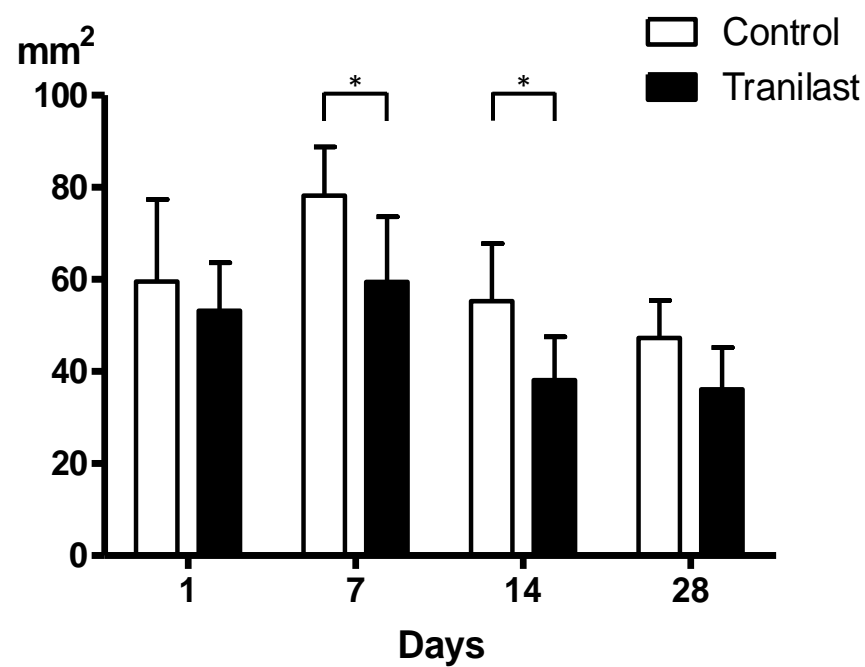
a

CT volumetry

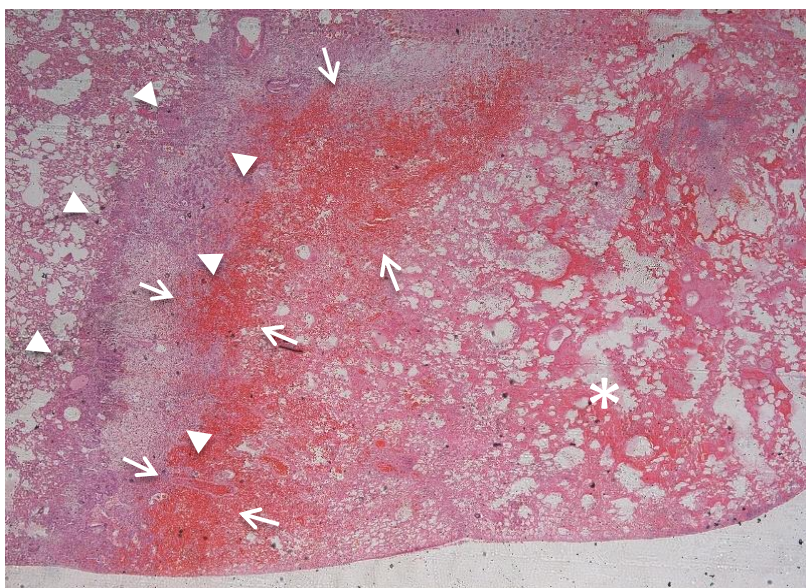


b

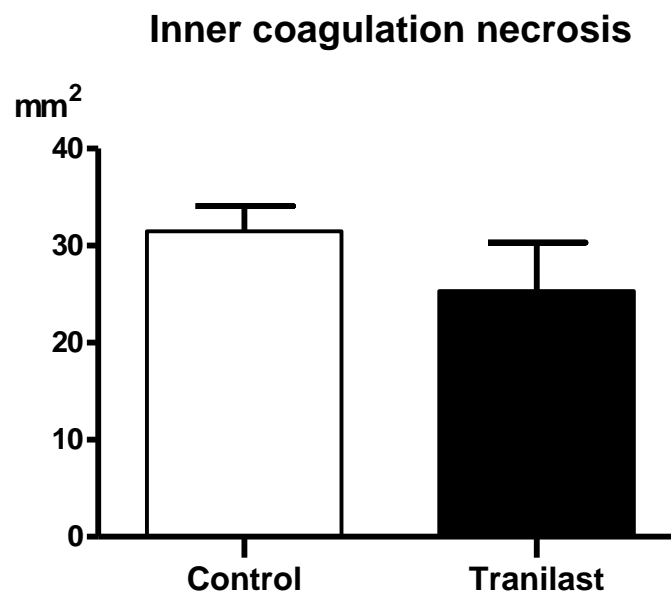
Pathological areas



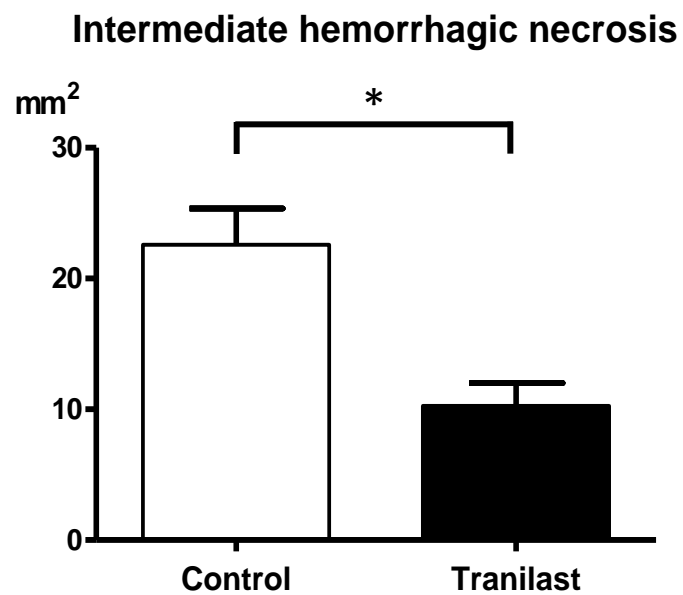
a



b



c



d

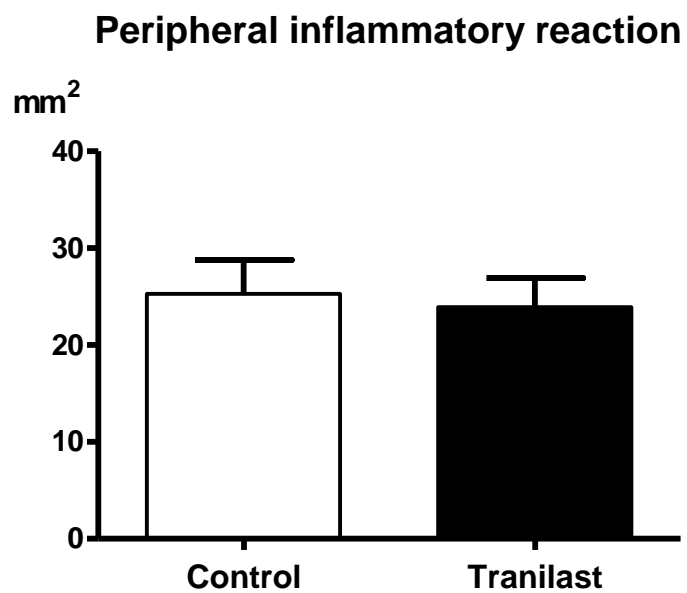
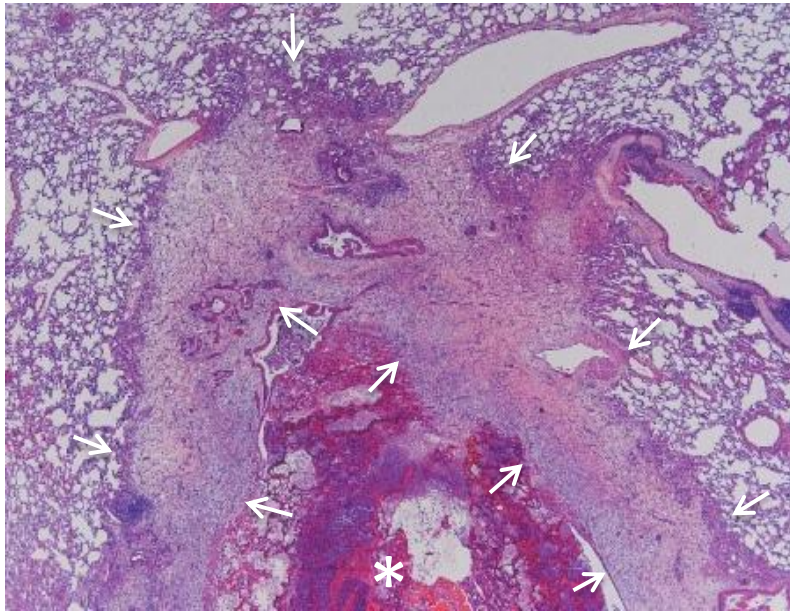


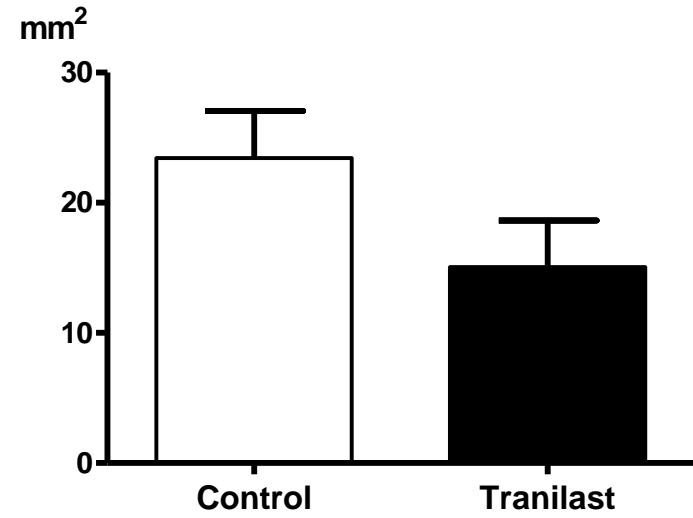
Figure 4

a



b

Coagulation necrosis mixed with hemorrhage



c

Peripheral inflammatory reaction

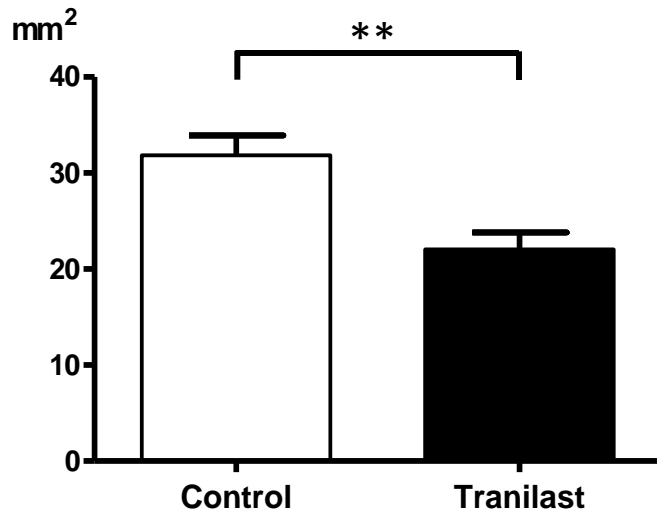
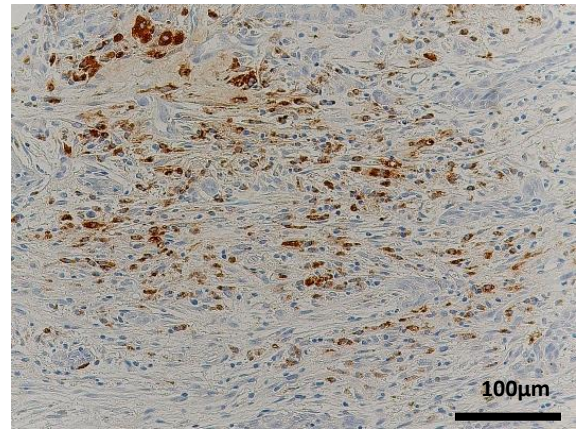
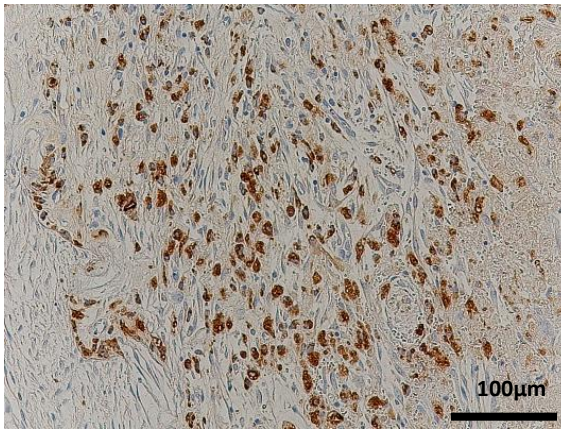


Figure 5

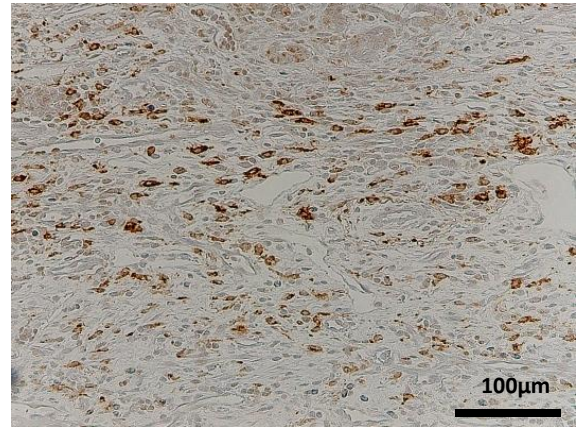
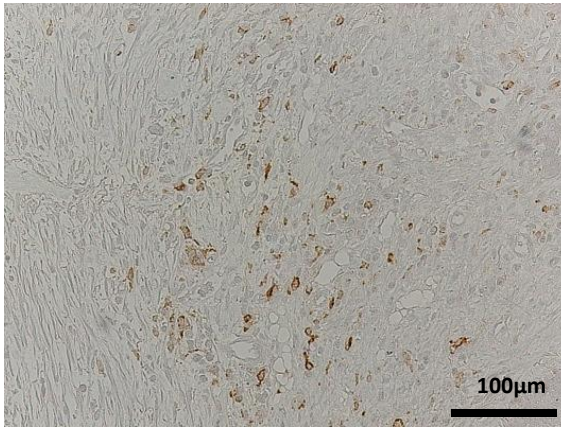
Control

Tranilast-treated

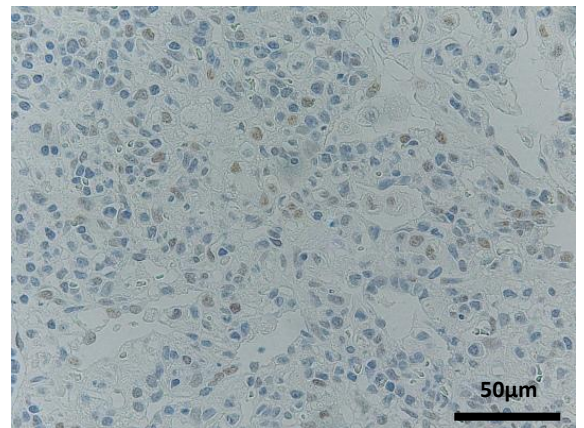
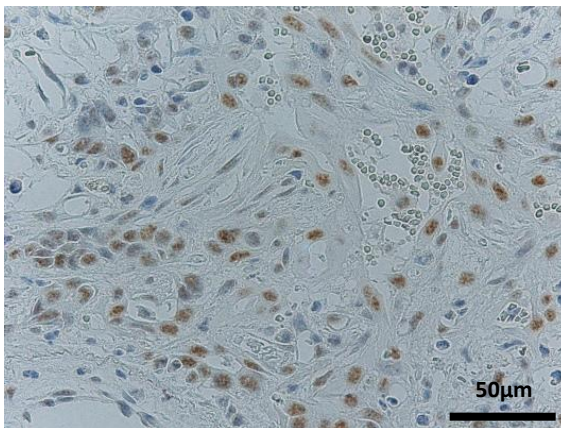
RAM11



CD163



NF-κB



CD31

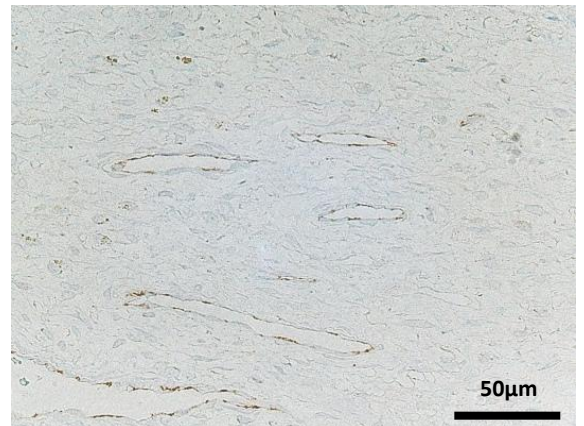
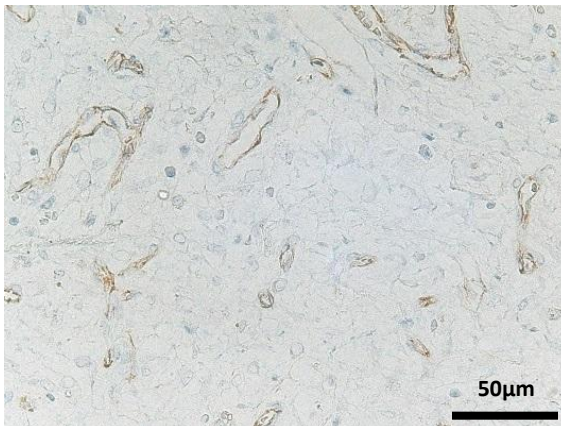
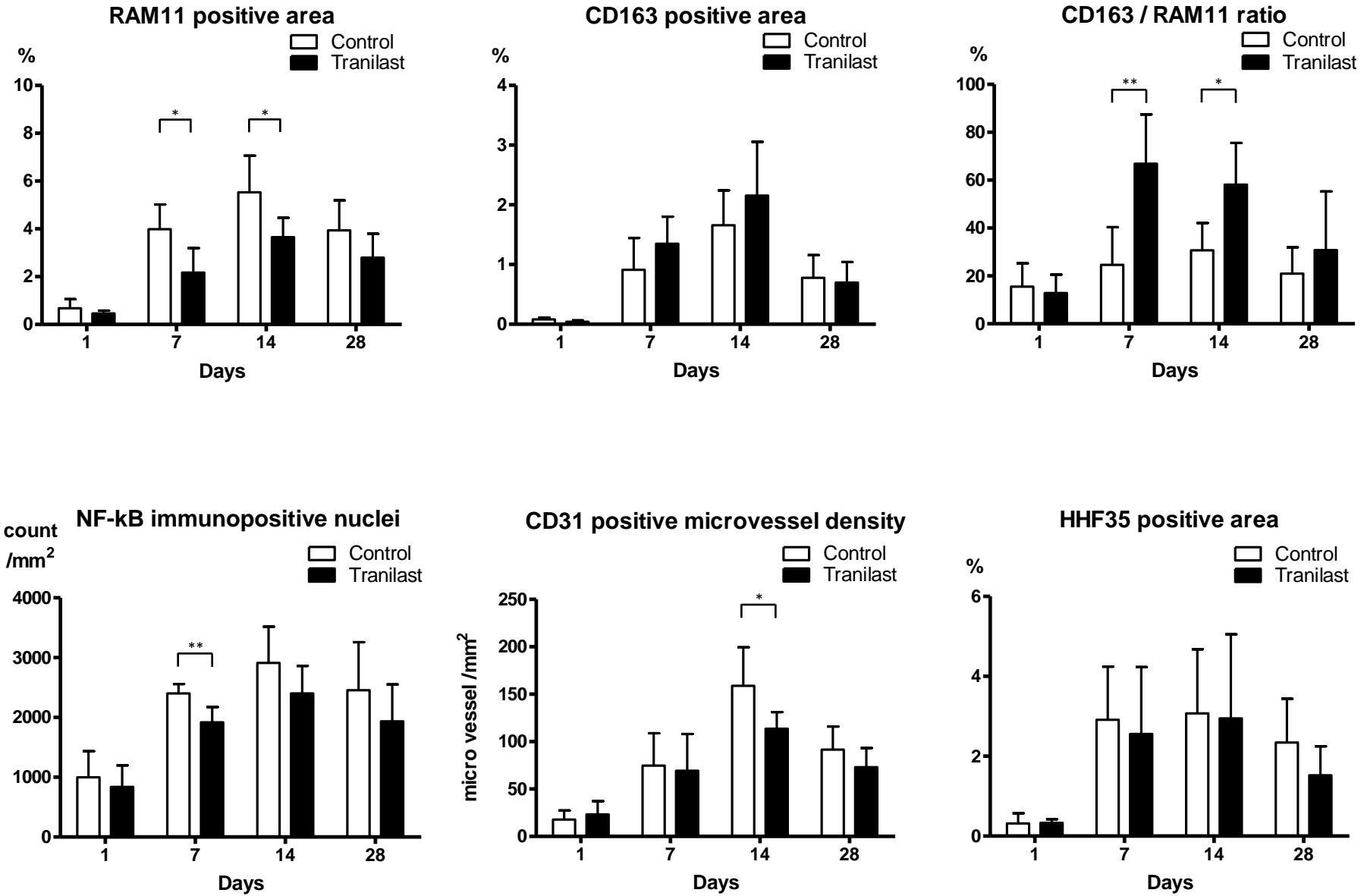


Figure 6



Acknowledgements

We are most grateful to Ms. Kyoko Ohashi, Ms. Ritsuko Sotomura, Ms. Yukiko Motoura, Ms. Tomoko Kawanami, Ms. Takako Sakamoto and Mr. Minoru Shiraishi for their technical assistance.